

Applied Tracking Control for Kite Power Systems

Claudius Jehle* and Roland Schmehl†
Delft University of Technology, 2629 HS Delft, The Netherlands

DOI: 10.2514/1.62380

This paper presents a tracking controller applicable to tethered flying objects, such as kites for power generation or towing purposes. A kinematic framework is introduced, employing definitions and terminology known from aerospace engineering, and is used for both modeling and control design. Derived from measurement data, an empirical steering-law correlation is presented, establishing a highly reliable connection between the steering inputs and the kite's yaw rate, and thus providing an essential part of the cascaded controller. The target trajectory is projected onto a unit sphere centered at the tether anchor point, and based on geometrical considerations on curved surfaces, a tracking-control law is derived, with the objective to reduce the kite's spacial displacement smoothly to zero. The cascaded controller is implemented and integrated into the software and hardware framework of a 20 kW technology demonstrator. Because of the lack of a suitable simulation environment, its performance is assessed in various field tests employing a 25 m² kite, and the results are presented and discussed. The results, on the one hand, confirm that autonomous operation of the traction kite in periodic pumping cycles is feasible; yet, on the other, that the control performance is severely affected by time delays and actuator constraints.

Nomenclature

B	= kite-fixed reference frame
C	= point on trajectory closest to kite position
c_1, c_2	= fitting coefficients of empirical yawing correlation
e_χ	= misalignment between the commanded and actual flight directions, error of inner loop
\mathbf{K}	= position of kite projected onto unit sphere
K_P	= proportional gain of inner-loop controller
\mathbf{O}	= tether anchor point and origin of wind reference frame W
p	= roll velocity of kite (cf. ω)
q	= pitch velocity of kite (cf. ω)
\mathbf{q}^K	= kite's azimuth- and elevation-angle tuple (ξ, η)
r	= yaw velocity of kite (cf. ω)
S	= local reference frame of tangent plane $T\mathbb{S}^2$
\mathbb{S}^2	= unit sphere around tether anchor point \mathbf{O}
${}^A\mathbb{T}_B$	= transformation matrix from reference frame $B \rightarrow A$
$T_{\mathbf{K}}\mathbb{S}^2$	= tangent plane to \mathbb{S}^2 at point $\mathbf{K} \in \mathbb{S}^2$
\mathbf{t}_C	= normalized course vector tangential to the target trajectory at closest point C
\mathbf{t}_K	= representation of course vector \mathbf{t}_C at the kite position \mathbf{K}
u_S, u_P	= relative steering/power setting
v_{app}	= apparent wind velocity
W	= wind reference frame

Greek symbols

β	= Kite's drift angle
δ	= geodesic distance between two points on unit sphere \mathbb{S}^2
$\delta^{C,K}$	= geodesic unit vector pointing from C to K along the geodesic connecting both points
δ_0	= turning-point distance (control parameter of bearing control loop)
η	= kite's elevation angle

Received 11 March 2013; revision received 19 July 2013; accepted for publication 19 July 2013; published online 12 February 2014. Copyright © 2013 by the authors. Published by the American Institute of Aeronautics and Astronautics, Inc., with permission. Copies of this paper may be made for personal or internal use, on condition that the copier pay the \$10.00 per-copy fee to the Copyright Clearance Center, Inc., 222 Rosewood Drive, Danvers, MA 01923; include the code 1533-3884/14 and \$10.00 in correspondence with the CCC.

*Former Graduate Student, ASSET Institute; currently Lenastraße 21, 12047 Berlin, Germany; c.jehle@jehle-rv.de.

†Associate Professor, ASSET Institute, Kluyverweg 1; r.schmehl@tudelft.nl.

θ	= second rotation angle of an Euler sequence (XYZ order) to convert $S \rightarrow B$
ξ	= kite's azimuth angle
ρ^C	= normalized position vector of C , closest point of \mathbf{K} on target track ρ_t^K
ρ^K	= normalized position vector of kite position \mathbf{K}
ρ_t^K	= normalized desired position vector of \mathbf{K} (i.e., the target track)
σ	= indicates whether \mathbf{K} is left (+1) or right (-1) with respect to the (directed) target track
ϕ	= first rotation angle of an Euler sequence (XYZ order) to convert $S \rightarrow B$
χ	= track angle, measured between \mathbf{x}_S and velocity vector of \mathbf{K}
$\chi_{C,K}$	= course angle between \mathbf{t}_K and \mathbf{x}_S at \mathbf{K}
χ_{cmd}	= bearing angle, commanded flight direction
ψ	= heading angle, last rotation angle of an Euler sequence (XYZ order) to convert $S \rightarrow B$
$\omega^{W,B}$	= angular-velocity vector of B reference frame relative to W

I. Introduction

ARBORNE-WIND-ENERGY (AWE) systems are designed to generate energy by means of tethered flying devices, such as wings or aerostats. Replacing the tower and rotor blades of conventional wind turbines by a lightweight tensile structure reduces, on the one hand, the investment costs and, on the other hand, decreases the environmental footprint. The low visual and acoustic impact is an advantage for installations in ecologically sensitive areas or tourist destinations, while the minimal weight and compact dimensions make the technology particularly attractive for mobile deployment. Because AWE systems operate at higher altitudes, they can access better wind resources, which can be used to increase the average availability of an installation.

An important class of concepts uses cable drums and connected generators on the ground to convert the traction power of tethered wings into electricity [1–4]. The essential advantages are that heavy system components can be positioned on the ground and that the wings can be optimized with respect to traction performance and controllability. Common single-kite concepts, such as the one presented in this paper, are based on operation in periodic cycles, alternating between reel out and reel in of the tether. During reel out, the traction force, and thus, the generated energy is maximized by flying the kite in fast crosswind maneuvers. The typical flight pattern is the lying figure of eight illustrated in Fig. 1, see also [5]. During reel in, the generator is operated as a motor and the kite is pulled back

toward the ground station. To minimize the amount of energy required for this retraction phase, the wing is depowered by decreasing its angle of attack. The two phases of the pumping cycle are illustrated in Fig. 2. For a small off-grid system, a rechargeable battery is used to buffer the energy over the periodic pumping cycles. For a group of interconnected systems, buffer capacity can be reduced by phase-shifted operation.

Compared to conventional tower-based wind turbines, the flight operation of a tethered wing can be adapted much further to the wind resource available at a specific location. For example, variations in the wind field can be compensated for by adjusting the altitude range of pumping cycles and making use of the fact that the wind gets generally stronger and more persistent with increasing altitude. Many other operational parameters can be modified on the fly to optimize the power output. Practical limits are imposed by the flight-dynamic

feasibility of specific trajectories, safety considerations, and airspace regulations.

The technical feasibility of AWE systems crucially depends on a robust and reliable flight control, and, as a matter of fact, the emerging renewable-energy technology has triggered a new and challenging research area. Several different methodologies for the automated control of traction kites have evolved. Optimal control approaches incorporate the additional objective of online optimization of the power output. The application of nonlinear model predictive control (NMPC) for traction kites was first proposed in [6] and expanded in [7–9]. The NMPC predicts the system behavior by means of a model, and generates a steering input signal such that a problem-specific cost function is optimized. For a power-generating traction kite, the cost function incorporates the maximization of the power output and stability criteria, for example, the condition that the kite does not exceed certain bounds of operation.

The NMPC approaches share the fact that they rely on system models to predict the flight-dynamic response of the kite to control inputs. Rigid-wing aircraft generally employ directional control surfaces, and the mechanism of steering is fairly well described by standard correlations between the control input and the induced aerodynamic forces and moments. Similar to parachute systems, inflatable traction kites are designed as tensile membrane structures. Flight control is implemented by pulling and releasing of steering lines, which change not only the geometry of the bridle system, but also induce a deformation of the wing. This mechanism has been investigated quantitatively by computational analysis based on high-resolution discretizations of the tensile membrane structure [10,11]. These simulations show that the turning behavior of C-shaped traction kites is affected substantially by the spanwise torsion of the wing, which amplifies the aerodynamic turning moments.

Another fundamental difference to rigid wings is the strong coupling of structural dynamics and exterior aerodynamics due to the low inertia and high flexibility of the inflatable wing. In essence, the shape during flight is defined by the dynamic equilibrium between the exterior flow and the resulting pressure distribution on the wing and the structural reaction forces [10,11]. This physical complexity is the reason for the high computational cost of high-fidelity modeling of the steering dynamics. In the framework of the NMPC, this leads to large and computationally expensive optimization problems. Additional hard constraints that are imposed on the problem increase the computational expenses even further. Thus, to profit from the advantages of the mathematically demanding and computationally intensive NMPC, it is necessary to perform further research on efficient high-fidelity modeling of inflatable traction kites.

Another control approach is based on evolutionary robotics (i.e., employing an evolution of neural network controllers using genetic algorithms [12]). Although this control methodology is particularly attractive due to its ability to adapt for changes, it is also rather complex. For safety reasons, evolutionary robotics are generally not employed for aircraft control. A nonlinear bang-bang controller for large traction kites for marine-transport application is presented in [13]. The approach makes use of an empirical correlation between the steering input and the yaw rate. A disadvantage of this method is the limited control authority: although the input command generates a figure-of-eight trajectory, the precise shape of this trajectory can only be adapted by advanced tuning at the command of the operators. Much effort is spent on circumventing the actuator constraints by smoothing the input signal. Although this protects the actuators, it eventually does not improve control performance.

A fourth approach is based on prescribed flight trajectories for maximum power output. The trajectories can either be precomputed on the basis of measured wind conditions, or they can be determined online using a trajectory planner. A Lyapunov-based control law combined with an online system identification and learning algorithm is presented in [14]. The implemented control law changes the flight direction of the kite in terms of its turning angle such that it smoothly aligns with the prescribed target trajectory.

Argatov and Silvennoinen [15] use the Frenet–Serret formalism to analytically model a tethered kite, and first point out the impact of the geometry of the kite's trajectory on the control problem.



Fig. 1 Crosswind figure-of-eight maneuver of a 25 m² tube kite ($\Delta t = 1$ s) [5].

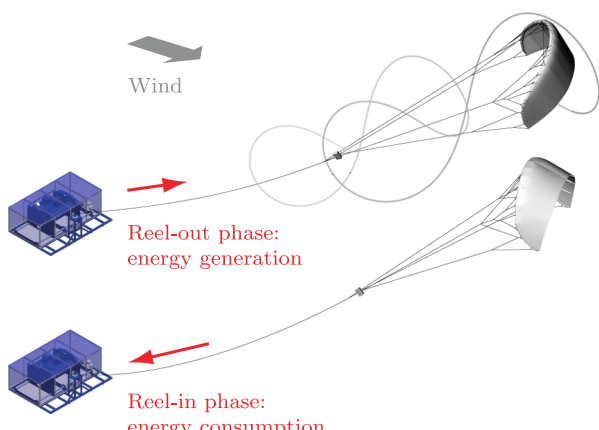


Fig. 2 Working principle of the pumping kite power system [2].

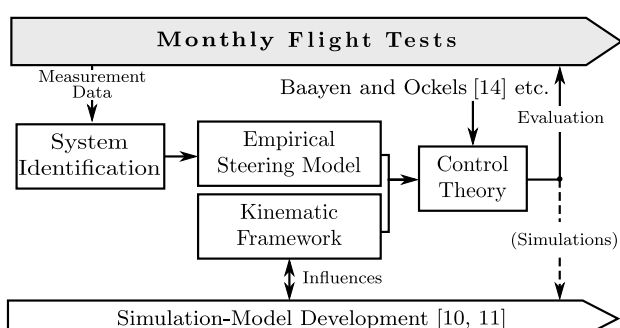


Fig. 3 Development process of the kite controller.

They elaborate the importance of the geodesic curvature, which will also play an important role in this paper.

The research presented in this paper builds upon the approach presented in [14]. Also, analogies to the Frenet–Serret framework in [15] are evident. However, while the base vectors of their tangent plane are coupled to the shape and curvature of the trajectory, here, a definition based on the formalism used in navigation and aerospace engineering, is used. The concept of the turning angle introduced in [14], here called track angle, and their coordinate systems are visualized and further substantiated by a kinematic framework tailored to tethered wings. The basic principle of this framework is to resemble well-known terminology and definitions from aerospace engineering, such as the employment of Euler angles for attitude description, the idea of leveled flight, and the tracking of a ground trajectory. This is described in Sec. III.C.

The adaptive-control component proposed by Baayen and Ockels [14], which turned out to be susceptible to dead times and actuator constraints, is replaced by an empirical system model (cf. Sec. III.B). It is then linearized using feedback linearization. Based on the kinematic framework presented in Sec. III.C and the prescription of a target trajectory, Sec. IV summarizes the derivation of a nonlinear tracking-control law, and its basic properties are described. Because of the lack of validated simulation models for kite power systems, this work focuses on the implementation of the controller in the 20 kW hardware demonstrator (cf. Sec. II), rather than drawing conclusions from a simulation. The controller proved its performance in various field tests, tracking the target trajectory with convincing accuracy and with a positive net-power output (cf. Sec. V). Figure 3 illustrates the design and development process of the presented controller.

II. System Setup

The technology demonstrator used for the research presented in this paper employs a 25 m^2 leading-edge inflatable (LEI) tube kite with a nominal traction force of 3.1 kN and a nominal traction power of 20 kW [2]. To minimize aerodynamic drag, which is an important system loss for a pumping kite power system, a single-line traction tether is used. Steering and depowering of the wing are implemented by an airborne kite control unit (KCU), which essentially is a cable robot suspended some 10 m below the wing. This setup is illustrated in Fig. 4. The traction tether is made of the high-strength plastic fiber Dyneema®. It has a diameter of 4 mm and a total length of 1 km, which can optionally be extended to 10 km. The main components of the inflatable C-shaped tube kite are the front tube, defining the curvature of the wing; the connected strut tubes, defining the wing profile; and the canopy. The function of the bridle-line system is to transfer the aerodynamic loading from the wing to the traction tether. As can be seen in Fig. 4, this line system realizes a distributed load transfer from the front tube. Included are the two steering lines, which attach to the rear ends of the wing tips and are actuated by the KCU. A combination of inertial measurement unit (IMU) and GPS is mounted to the middle strut of the wing, as visible in Fig. 4.



Fig. 4 KCU suspended below the 25 m^2 inflatable wing [16].

Communication between the ground station and the KCU board computer is established by two redundant wireless links [16]. The system control software runs on a ground computer, and uses the control positions and status of the actuators transmitted from the KCU and the IMU–GPS module. The software distinguishes between two control modes associated with the two phases of the pumping cycle: a figure-of-eight trajectory control during reel out, which is presented in this paper, and a zero-azimuth stabilization controller during reel in.

An important feature of the development platform is the logging of all measurement data together with the video streams of various cameras at the ground station, the kite, and the KCU. These data are used to analyze and improve the flight dynamics and structural dynamics of the kite, as well as the performance of the complete kite power system.

III. System Model

As mentioned in the Introduction of this paper, the flight dynamics and mechanism of steering of inflatable traction kites are governed by strong two-way coupling of structural dynamic and aerodynamic processes. One approach to model an inflatable tube kite supported by a complex bridle system is based on discretization as a multibody system [10,17]. This structural model represents the inflatable tubular frame with leading edge and connected struts by joined rigid body elements. The canopy fabric is represented as a two-dimensional matrix of spring–damper elements, whereas the bridle lines and the tether are modeled as rigid line elements. To maintain a high computational efficiency, this structural model is combined with a parametric model for the distributed aerodynamic wing loading. The required shape parameters chord length, camber, and thickness are determined per wing section. The aerodynamic wing-loading model is used in combination with a finite element representation of the wing [11]. Both authors investigate the mechanism of steering for C-shaped membrane kites, and essentially confirm the importance of wing torsion deformation and local deformations induced by variations of the aerodynamic load for cornering maneuvers.

These models help to understand the fundamentals of the flight dynamics of kites, and are essential for optimizing and improving wing shape, actuation, and, eventually, the power output. However, the high-degree-of-freedom (DOF) discretization due to the fine-mesh resolution and the complex aerodynamic models leads to considerably high computational effort and long simulation times. Moreover, even models that have been synthesized using system-reduction approaches, resulting in reduced amount of DOF, still contain a reasonable amount of parameters, such as inertial properties and aerodynamic coefficients [18], that have to be determined by excessive system-identification efforts. These constraints limit their immediate use for the purpose of controller design. As the kite research group of Delft University of Technology has a working kite power system available, and all important input and output values are measured, the research objective was to investigate the input–output problem from an empirical point of view. As a result, a good fit between the measurement data and the black-box model has been achieved. The company SkySails independently presents a slightly different correlation for much bigger kites in [13], which supports the validity of the black-box model.

The correlation presented is strongly supported by measurement data, and establishes a connection between the steering input u_S and the yaw rate r_B . This yaw rate is the body-fixed rotational rate of the kite around its \mathbf{z}_B axis, which also appears as the third component of the angular-velocity vector $(\boldsymbol{\omega}^{WB})_B$. The steering input u_S gives a relative measure for the difference in steering-line length between the two wing tips, so that $u_S = \pm 100\%$ refers to full pulling on the right (left) side. See Fig. 5 for an explanation of the steering-line setup and the bridle system. Beside the steering input u_S , there is also the power setting $u_P \in [0 - 100\%]$, which is linked to the angle of attack of the kite. A powered kite has a power setting $u_P \approx 60\text{--}100\%$, which equates to a high angle of attack, whereas a depowered kite usually has a $u_P \leq 40\%$. Both states of the wing are illustrated in Fig. 6.

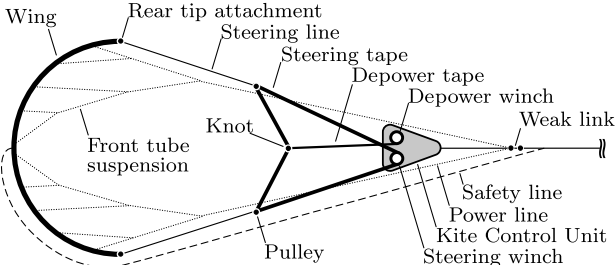


Fig. 5 Schematic of bridle and steering system.

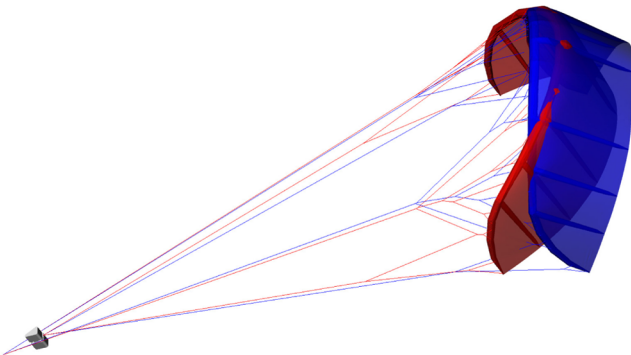


Fig. 6 Powered (red) and depowered (blue) states of the kite.

A. Kinematic Framework

In aerospace engineering, it is common practice to describe the attitude of airplanes using *XYZ*-type Euler angles [19] between a northeast-down (*NED*)-type earth-fixed reference frame and the body-fixed reference frame of the flying vehicle. One advantage is that, in leveled flight, the kinematical equations of the planes are decoupled to a large extent and have a simple form, which facilitates, for example, the implementation of flight-control algorithms. The notation of a vector $(\mathbf{v}_B^A)_C$ comprises its physical direction *A* and additional information *B*. When used in the context of a reference frame *C*, the containing reference frame is denoted outside the brackets.

A similar framework, based on a spherical coordinate system centered at the tether anchor point **O**, is proposed for tethered wings. This framework is based on the definitions known from aerospace, and, with only minor changes, most techniques from navigation and aerospace engineering are applicable.

1. Reference-Frame Definition

Because of the tethering, kites usually fly at a certain elevation angle relative to their ground station, and are thus not leveled out in respect to the ground surface. In terms of the aforementioned Euler angles, the kite's bank and pitch angles are hence neither negligible nor are the attitude kinematic equations decoupled, which unnecessarily complicates the control-design process.

To work around this problem, a new reference for the attitude representation is introduced. Just like a plane flies above the earth surface, with gravity being the major force to counteract, a kite can be seen as flying above an imaginary spherical surface, wrapped around the tether anchor point **O**. The major force acting on a kite is the tether force, which is always directed along the tether, as it has no bending stiffness. Gravity plays only a minor role, because the aerodynamic forces are larger by magnitude (in particular in the traction phase). This unit sphere, denoted by \mathbb{S}^2 , can be interpreted as a small earth, and several analogies of a plane flying over the ground surface can be applied. Among those are 1) description of the kite's position in spherical coordinates relative to a wind-fixed reference frame, 2) description of the kite's attitude with Euler angles relative to a reference frame based in a tangent plane of \mathbb{S}^2 , and 3) prescription of a target trajectory \mathbb{S}^2 .

The wind reference frame *W*, centered at **O**, has its \mathbf{x}_W axis pointing downwind, and \mathbf{z}_W is pointing up. It resembles the Earth-centered, Earth-fixed (ECEF) coordinate system, in which longitude and latitude are used to describe an object's position, here referred to as azimuth and elevation angles. Note that, during field tests, it became a common practice for the ground operators to count ξ positively to the right-hand side (west), unlike the ECEF longitude, which is positive to the east. To avoid confusion with the later-introduced Euler angles, these angles are denoted by ξ and η , respectively. Moreover, as the remainder of this paper will only deal with the kite's tracing point **K** on \mathbb{S}^2 , the indication of the constant unit distance becomes obsolete.

The conversion between the Cartesian representation $\rho^K \in \mathbb{R}^3$ and the spherical angles $\mathbf{q}^K = [\xi, \eta]^T \in [-(\pi/2), +(\pi/2)] \times [0, +(\pi/2)]$ can be found in the Appendix. The tracing point **K**, which is basically the intersection of the kite's position vector with \mathbb{S}^2 , supports the local tangent plane $T_K \mathbb{S}^2$, which in turn contains the reference frame *S*. As shown in Fig. 7, \mathbf{x}_S is pointing upward along the local meridian, resembling Earth's north direction, whereas \mathbf{z}_W points inward. The attitude of the kite, represented by the kite-fixed reference frame *B*, is now given by a set of Euler angles $\{\phi, \theta, \psi\}$ (*XYZ* order), relative to *S* rather than to *W*, conformal to the common aerospace definition. *B* is defined as follows: \mathbf{y}_B from left to right wing tip and \mathbf{z}_B downward, parallel to the tether. All reference frames are right handed.

This contrivance leads to most widely decoupled attitude dynamics, and while the heading angle ψ can almost directly be used as an input to the later-presented tracking controller, the pitch and bank angles θ, ϕ give a measure for the straightness of the tether. $\theta = \phi = 0$ equates to a straight tether, whereas nonzero values imply a tether sag, as shown in Fig. 8.

A coordinate transformation from *S* to *B* is performed using an *XYZ*-order transformation matrix ${}_B \mathbb{T}_S$ (${}_S \mathbb{T}_B = {}_B \mathbb{T}_S^T$), which can be found in any appropriate flight-dynamic book (e.g., [19]). The component transformation of any vector in *W* to *S* is achieved by a *YXY* sequence of $\{-(\pi/2), -\xi, -\eta\}$:

$$\begin{aligned} {}_S \mathbb{T}_W &= \mathbf{R}_y(-\eta) \mathbf{R}_x(-\xi) \mathbf{R}_y(-\pi/2) \\ &= \begin{bmatrix} -\sin \eta \cos \xi & \sin \eta \sin \xi & \cos \eta \\ \sin \xi & \cos \xi & 0 \\ -\cos \eta \cos \xi & \cos \eta \sin \xi & -\sin \eta \end{bmatrix} \quad (1) \end{aligned}$$

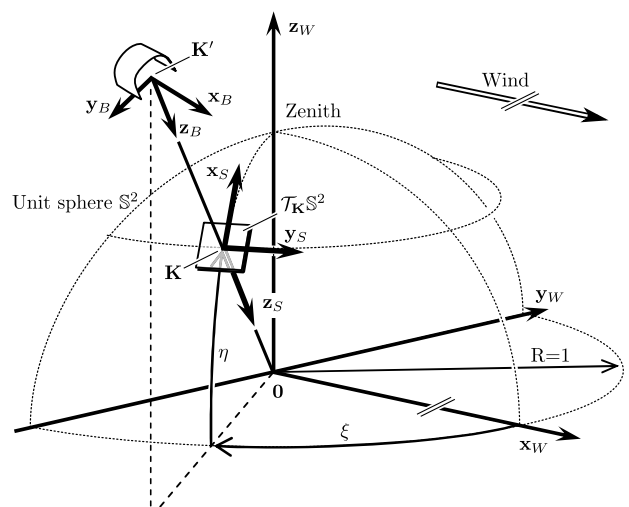


Fig. 7 Visualization of the kinematic framework proposed for tethered airborne systems.

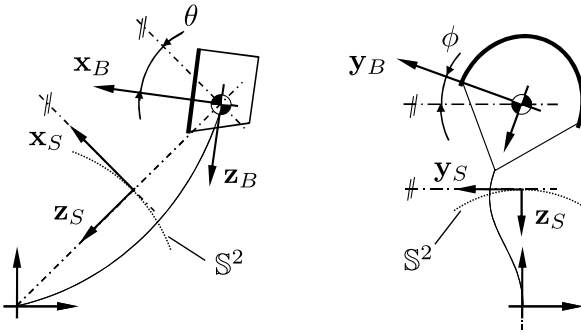


Fig. 8 A measure for the tether sag, $\theta = \phi \neq 0$ corresponds to a nonstraight tether.

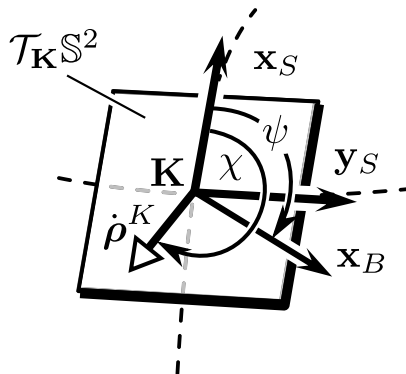


Fig. 9 Local tangent plane with essential vector and angle definitions.

such that $(\mathbf{v})_S = {}_S \mathbb{T}_W \cdot (\mathbf{v})_W$ (see [20] for details). Note the similarity of this matrix to the one of a transformation between the ECEF and a NED basis of a tangent plane to Earth, replacing ξ by the longitude and η by the latitude angle.

2. Angle Definitions

The heading angle ψ quantifies in which direction relative to \mathbf{x}_S the kite's nose is pointing. This is also depicted in Fig. 9. However, the heading and the actual flight direction can be misaligned. This misalignment in turn is quantified by the track angle (called turning angle in [14], and defined between what is here \mathbf{y}_S and the projected flight direction), defined as the angle between \mathbf{x}_S and the velocity of \mathbf{K} , $\dot{\rho}^K \in \mathcal{T}_K \mathbb{S}^2$ ($\|\dot{\rho}^K\| =: \dot{\rho}^K$):

$$\chi := \cos^{-1} \left(\frac{\mathbf{x}_S \cdot \dot{\rho}^K}{\dot{\rho}^K} \right) \in [0, 2\pi] \quad (2)$$

The difference between ψ and χ is the drift angle (in aerospace-engineering terminology, sometimes referred to as kinematic sideslip angle):

$$\beta = \chi - \psi \quad (3)$$

3. Rotational Dynamics

The kite's angular-velocity vector relative to the wind reference frame can be decomposed into two independent rotations. According to [21], which gives a very detailed and universal overview of the representation of attitudes, the decomposition is linear: $\boldsymbol{\omega}^{WB} = \boldsymbol{\omega}^{WS} + \boldsymbol{\omega}^{SB}$. The first term on the right-hand side contains the rotation of the basis S of $\mathcal{T}_K \mathbb{S}^2$ as it moves on \mathbb{S}^2 , whereas the second term expresses the change of orientation of the kite-fixed reference frame B relative to S .

Expressing the angular velocities of the kite relative to the fixed reference frame W yields (in B coordinates)

$$(\boldsymbol{\omega}^{WB})_B = \begin{bmatrix} p_B \\ q_B \\ r_B \end{bmatrix} = {}_B \mathbb{T}_W \cdot \begin{bmatrix} 0 & -\sin \xi \\ 0 & -\cos \xi \\ -1 & 0 \end{bmatrix} \cdot \begin{bmatrix} \xi \\ \dot{\eta} \end{bmatrix} + \begin{bmatrix} -\sin \theta & 0 & 1 \\ \cos \theta \sin \phi & \cos \phi & 0 \\ \cos \theta \cos \phi & -\sin \phi & 0 \end{bmatrix} \cdot \begin{bmatrix} \dot{\psi} \\ \dot{\theta} \\ \dot{\phi} \end{bmatrix} \quad (4)$$

Both terms can be taken from, for example, [20].

B. Empirical Steering Correlation

Figure 10 depicts the components of $(\boldsymbol{\omega}^{WB})_B$ together with the steering input u_S for one figure of eight during powered flight. During the first 62 s, the power setting was set to $u_P = 80\%$, leading to a high angle of attack and likewise high tether forces. While both roll p_B and pitch rate q_B are negligibly small and seem unaffected by the steering input, the yaw rate r_B significantly varies; an almost linear correlation $r_B \propto u_S$ can be observed. From $t > 62$ s, the kite is being depowered by reducing the power setting to $u_P = 40\%$ (power setting not plotted), leading to low tether forces and a slack kite. Although the (in this case, human) operator further applies steering inputs of the same magnitude, hardly any reaction of the kite is observable. A depowered kite is almost unmaneuverable, and shall therefore at first be out of our focus.

A curve-fitting approach to link r_B to u_S was performed in time domain, using the following base equation:

$$r_B = c_1 v_{app} u_S + c_2 \frac{\mathbf{g} \cdot \mathbf{y}_B}{g} \quad (5)$$

A very good fit was achieved for sufficiently high tether forces (i.e., as long as u_P was set sufficiently high). The result of the identification is shown in Fig. 11 for three consecutive figures of eight. The equation shows interesting similarities to the one found in [13] for ram-air kites; however, without the reciprocal dependency on v_{app} in the second term. Moreover, the validity of correlation has also been supported by the simulation work of Bosch [11]. The parameters c_1 ,

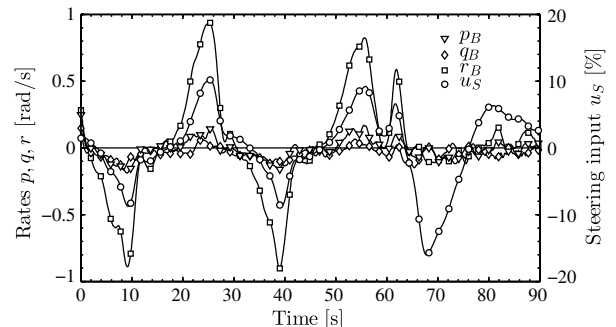


Fig. 10 Evolution of the body-fixed angular rates when applying a steering input u_S .

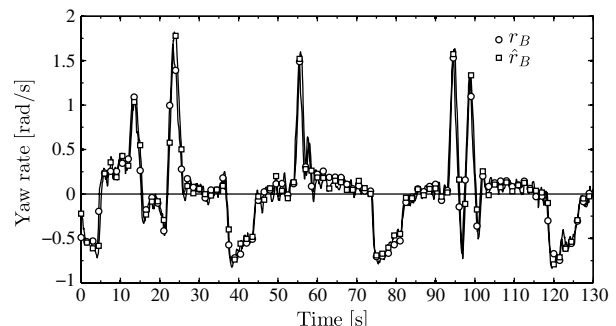


Fig. 11 Evaluation of Eq. (5) with $c_1 = 0.153$, $c_2 = 0.250$ for a 25 m^2 LEI kite.

$c_2 \in \mathbb{R}$ are kite specific. The coefficient c_1 seems to depend on the kite's geometry and mass, as well as the power setting, which affects the kite's angle of attack. A higher angle of attack will lead to higher c_1 , which reflects the observation that, given the same steering input, a fully powered kite reacts much more rapidly than a depowered one.

The second term of Eq. (5) takes into account the gravitational effects. In this equation, $\mathbf{g} \cdot \mathbf{y}_B$ gives a measure for the angle between gravity \mathbf{g} and the \mathbf{y}_B axis of the kite-fixed reference frame. It is believed that a kite flying a crosswind maneuver needs a slight steering offset, resulting in different angles of attack of the wing tips, to generate a lift force to counteract gravity. An equilibrium of forces of the resulting upward lift and downward gravity is established.

While the evaluation of the correlation is promising, some questions remain. It is interesting that v_{app} appears linearly, as the dependency of aerodynamic forces and moments on v_{app} is to the power of 2. Research is carried out to investigate these questions and to give analytical expressions for the parameters c_1 and c_2 , and the authors hope to be able to present physical interpretations in the near future.

In the following, the focus is put on the utilization of this correlation for the purpose of control, and it is referred to future publications regarding the interpretation of the correlation.

C. Summary

To control the position of a kite and make it track a target trajectory, which will later be prescribed on \mathbb{S}^2 , control of its direction of motion is necessary. With the aid of the previous subsections, a connection between this direction, represented by the track angle χ [cf. Eq. (2)], and the steering input u_S can now be established. This input/output connection forms the core of the controller.

Inserting Eq. (30) into the third row of Eq. (4) yields

$$r_B = -\dot{\rho}^K \sin \chi \tan \eta + \dot{\psi} \cos \theta \cos \phi - \dot{\theta} \sin \phi \quad (6)$$

The first term stems from the rotation induced by the tether constraint, whereas the others arise from evaluating the rightmost matrix multiplication in Eq. (4). Comparing that to the empirical yaw correlation in Eq. (5), and using Eq. (3) result in

$$\dot{\chi} = \frac{1}{\cos \theta \cos \phi} \left[c_1 v_{app} u_S + c_2 \frac{\mathbf{g} \cdot \mathbf{y}_B}{g} + \dot{\rho}^K \sin \chi \tan \eta - \dot{\beta} \cos \theta \cos \phi + \dot{\theta} \sin \phi \right] \quad (7)$$

which expresses the change of the track angle in terms of the steering input. This rather longish equation can be simplified to a great extent by two assumptions:

1) Straight tether: Field tests show that, during powered flight, the tether is an almost perfectly straight line. Compared to the tether forces ($F_t \approx 1 - 5$ kN), gravity plays a minor role ($F_g \approx 0.1$ kN), and it is thus assumed that these tether forces are sufficiently high to straighten out the tether. This relates to $\phi = \theta \approx 0$ (see also Fig. 8).

2) Low drift: It is assumed that the difference between the flight direction and heading [β , see Eq. (3)] is low, and that its evolution in time $\dot{\beta}$ can be neglected. This assumption also needs to be made, as a dynamic model for the drifting behavior is not yet available.

The validity of these assumptions will be discussed in Sec. V of this paper. Besides the fact that most trigonometric terms drop out due to the first assumption, the term $\mathbf{g} \cdot \mathbf{y}_B$ can be expressed as

$$(\mathbf{g})_W \cdot {}_W \mathbb{T}_B \cdot (\mathbf{y}_B)_B \approx g \sin \psi \cos \eta \quad (8)$$

by aid of Eq. (1). Reinserting into Eq. (7) yields

$$\dot{\chi} = c_1 v_{app} u_S + \sin \chi (c_2 \cos \eta + \dot{\rho}^K \tan \eta) \quad (9)$$

This simplified version of Eq. (7) will be the basis for the controller design, which will be treated in the following subsection.

IV. Control Strategy

The demand to fly prescribed trajectories (e.g., the previously mentioned figures of eight) motivates the development of a trajectory controller minimizing the distance between the kite and the target track. It is known from [22] that the mechanical power available from the AWE generation can be estimated by

$$P_m \approx F_T \cdot v_r \quad (10)$$

in which F_T is the tether force, and v_r is the reeling velocity. F_T can be maximized by wide trajectories (i.e., high crosswind components) at low elevation angles, while the reeling velocity v_r determines the stretching of the trajectory in the outward direction. The proposed control structure splits the task of optimizing the power output and delegates the control of the reel velocity to the winch controller (not in the scope of this paper), so that the tracking task reduces to a two-dimensional one. Both positions of the kite and target trajectory are projected onto the surface of the unit sphere \mathbb{S}^2 , and a cascaded controller controls the track angle χ of the kite to minimize the distance between the projected kite position and the target track.

A. Geometrical Considerations

Let the target trajectory $\rho_t^K(s): \mathbb{R} \rightarrow \mathbb{R}^3$ be prescribed on \mathbb{S}^2 and parameterized by the arc length s , and let s_C be the parameter of a point \mathbf{C} on ρ_t^K , so that

$$\rho_t^K(s = s_C) = \rho^C \hat{=} \mathbf{C} \quad (11)$$

Point $\mathbf{C} \in \mathbb{S}^2$ needs to be chosen, such that it has the shortest geodesic distance δ to \mathbf{K} ; in other words, the length of the path that connects both points on the surface of \mathbb{S}^2 is minimal, as it is also depicted in Fig. 12. This path is called geodesic, and its arc length can be calculated by [14,23]

$$\delta = \cos^{-1}(\rho^K \cdot \rho^C) \quad (12)$$

To find the parameter s_C such that $\delta \rightarrow \min$, the following equations have to hold:

$$\frac{\partial \delta}{\partial s} \Big|_{s_C} = 0, \quad \frac{\partial^2 \delta}{\partial s^2} \Big|_{s_C} > 0 \quad (13)$$

When implementing the controller, this task can either be done by a numerical optimization or analytically; yet, as this section focuses on the derivation of the control law, this problem is not further addressed. Assume s_C has been found, and then evaluating the first condition yields

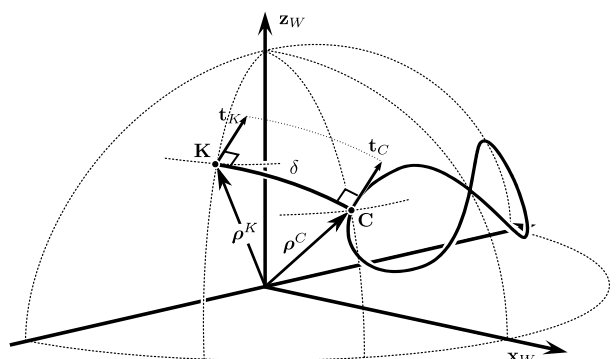


Fig. 12 Depiction of the geodesic and the tangent vector \mathbf{t}_C .

$$\left. \frac{\partial \delta}{\partial s} \right|_{s_C} = -\frac{\rho^K}{\sin \delta} \cdot \overbrace{\left. \frac{\partial \rho^K}{\partial s} \right|_{s_C}}^{\text{:=t}_C} = -\delta^{CK} \cdot \mathbf{t}_C = 0 \quad (14)$$

in which \mathbf{t}_C is the course vector tangential to the target track at point C. From this equation, δ^{CK} is the geodesic vector pointing along the geodesic toward K:

$$\delta^{CK} = \frac{\rho^K - \cos \delta \cdot \rho^C}{\sin \delta} \in \mathcal{T}_C \mathbb{S}^2 \quad (15)$$

The right-hand side of Eq. (14) follows from inserting Eq. (15) and noting that $\rho^C \perp \mathbf{t}_C$, and shows that the geodesic intersects the target trajectory perpendicularly. Computing the total time derivative of δ yields

$$\dot{\delta} = \frac{-1}{\sin \delta} (\dot{\rho}^K \cdot \rho^C + \dot{s} \overbrace{\rho^K \cdot \mathbf{t}_C}^{=0,(14)}) = -\dot{\rho}^K \cdot \delta^{KC} \quad (16)$$

The decrease of the geodesic distance is hence just that amount of the projected kite velocity that points along the geodesic. This is also visualized in a conformal map, Fig. 13, in which the situation has been unrolled along the geodesic. All vectors maintain their orientation relative to the geodesic.

For the case $\rho^K = \rho^C$, the geodesic distance δ is 0, and hence Eq. (15) is undefined. Moreover, if the kite crosses the track, the geodesic vector δ^{CK} flips by 180 deg. Therefore, σ is introduced, which indicates whether the kite is left (+1) or right (-1) of the target track:

$$\sigma = \begin{cases} +1, & \rho^C \cdot (\mathbf{t}_C \times \delta^{CK}) > 0 \\ -1, & \rho^C \cdot (\mathbf{t}_C \times \delta^{CK}) < 0 \\ 0, & \text{otherwise} \end{cases} \quad (17)$$

By the aid of Fig. 13, the geodesic vector can be expressed in the S basis at K as

$$(\delta^{KC})_{S,K}^\top = \left[\cos(\chi_{C,K} + \sigma \frac{\pi}{2}) \quad \sin(\chi_{C,K} + \sigma \frac{\pi}{2}) \quad 0 \right]$$

in which $\chi_{C,K}$ is the angle between $\mathbf{x}_{S,K}$ at K and the course vector \mathbf{t}_K . It is referred to as course angle to distinguish it from the track angle χ . Evaluating Eq. (16) in the S basis yields

$$\dot{\delta} = -\sigma \dot{\rho}^K \sin(\chi - \chi_{C,K}) \quad (18)$$

This scalar equation shows that the decrease of the geodesic distance depends on the kite's projected velocity (magnitude $\dot{\rho}^K$ and orientation χ), but also on the shape of the target trajectory at the projected kite position K, represented by $\chi_{C,K}$. Hence, to drive the geodesic distance toward zero, both the controllability of χ and knowledge of $\chi_{C,K}$ is necessary. The controllability of χ was already shown in Eq. (9), and will be further addressed in Sec. IV.B.

The determination of the course angle $\chi_{C,K}$, however, requires some attention. For any given target trajectory ρ^K_t , the closest point C and the adjacent course vector \mathbf{t}_C are determined using the mathematical framework presented earlier in this section. Calculating the course angle $\chi_{C,C}$ at C is a straightforward task; yet, as emphasized before, knowledge of $\chi_{C,K}$ at K is necessary. Interpret this as the shape of the track at K. The course vector \mathbf{t}_K needs to be transported from its origin at C to K, and as Fig. 13 already indicates, both course vectors need to maintain their relative (perpendicular) orientation relative to the geodesic. This, however, is not true for $\mathbf{x}_{S,K}$ and $\mathbf{x}_{S,C}$, so that in general, $\chi_{C,C} \neq \chi_{C,K}$.

Mathematically, transportation of \mathbf{t}_C to K is achieved, performing an active rotation about the axis $\rho^K \times \rho^C$ by δ , for which, for example, the Rodrigues formula [21] can be employed:

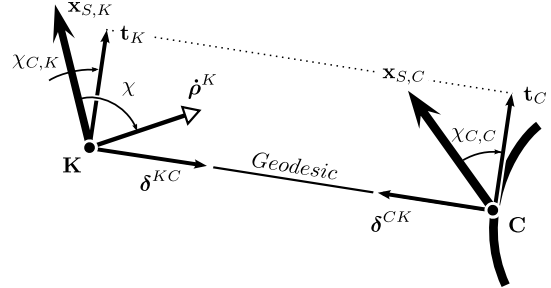


Fig. 13 Conformal map (preserving angle information) of the geodesic and the relevant angles.

$$\mathbf{t}_K = {}_K \mathbb{P}_C \cdot \mathbf{t}_C \quad (19)$$

In contrast to a coordinate transformation \mathbb{T} , this is an active operation, affecting the actual vector. The operator ${}_K \mathbb{P}_C$ maps a vector from one tangent space at C to K:

$${}_C \mathbb{P}_K : \mathcal{T}_C \mathbb{S}^2 \rightarrow \mathcal{T}_K \mathbb{S}^2$$

As this rotation preserves the orientation relative to the transport path (in this case, the geodesic), and $\delta^{CK} \perp \mathbf{t}_C$ [Eq. (14)], it also follows that $\delta^{KC} \perp \mathbf{t}_K$.

B. Feedback Linearization

According to Eq. (9), there is access to the track angle via the steering input u_S . As this equation, however, contains a series of nonlinear dependencies on the elevation angle η , and due to the fact that $\chi \in [0, 2\pi]$ can hardly be linearized at one specific operation point, it cannot be used for a linear controller. Yet, by rearranging one yields the steering input u_S^{cmd} necessary to achieve a desired rate $\dot{\chi}_d$:

$$u_S^{\text{cmd}} = \frac{1}{c_1 v_{\text{app}}} [\dot{\chi}_d - \sin \chi (c_2 \cos \eta + \dot{\rho}^K \tan \eta)] \quad (20)$$

This serves as a linearizing feedforward block, as with perfect knowledge of c_1 , c_2 and all other values measurable, both Eq. (20) together with the plant result in a linear integrator.

In fact, Eq. (20) is a simple form of a nonlinear dynamic inversion with relative degree one (with the output defined as χ), for which any linear or nonlinear controller can be designed. To be able to perform a full feedback linearization, all dynamic terms (i.e., $\dot{\rho}^K$, v_{app} , η and their dependency on u_S) have to be taken into account, and the stability of the inner dynamics has to be proved. However, integrating these states at this stage of system knowledge (i.e., the lack of a system model and especially the unknown influence of the steering input on other states than the yawing behavior) would be a rather speculative operation. Yet, as all values $\dot{\rho}^K$, v_{app} , η are position dependent and evolve much slower than the attitude dynamics, their dependency on the steering input u_S was neglected in the inversion. From a control point of view, these values turn into disturbances, which are fortunately measurable by means of a positioning system.

An issue that has to be addressed is the quality of the inversion. The parameters c_1 , c_2 may not be known or possibly changing under certain conditions; the measured values may be distorted by faulty measurement data; and the actuators might be incapable of performing the required steering inputs u_S^{cmd} , resulting in $\dot{\chi} \neq \dot{\chi}_d$. One way to face this issue is to add a (slow) loop $C(s)$ (e.g., a proportional-integral (PI) compensator) penalizing the error $e_l = \dot{\chi}_d - \dot{\chi}$, so that $\dot{\chi}_d = \dot{\chi} + C(s) \cdot e_l$. In case of matching $\dot{\chi}_d$, $\dot{\chi}$, no additional control effort is needed; only if the linearization model differs from the real plant a correction term is superimposed. However, $\dot{\chi}$ should be measurable to avoid numerical differentiation. The yaw rate r_B (which is usually measured by IMUs) can be used for this purpose.

A more elaborate approach is to augment the inversion with an adaptive element designed to either perform an online system

identification for c_1, c_2 (cf. [14]) or to directly compensate for uncertainties by comparing the performance of the inversion with a reference model (model-reference adaptive control (MRAC) [24]). The derivation of an adaptive-control law is however beyond the scope of this work, although experiments have been carried out with an MRAC law. The main challenge for the adaptive-control law is the susceptibility of this approach to actuator constraints and dead time. The incorporation of those is still subject to research (e.g., pseudocontrol hedging [25]). Thus, for the derivation of the linear controller (next subsection), a perfect inversion is assumed, and the robustification of the inversion is postponed to future research.

C. Control Structure

1. Bearing Controller

Recall from Eq. (18) that the geodesic distance can be decreased by controlling the track angle χ . Let now

$$\dot{\chi}_{\text{cmd}} := \dot{\chi}_{C,K} + \tan^{-1}\left(\sigma \frac{\delta}{\delta_0}\right) \quad (21)$$

be the bearing angle (i.e., a desired flight direction of the kite). For large distances, the \tan^{-1} term assumes values close to 90 deg, and hence the bearing would point perpendicular to the target track. For small distances, it approaches zero, leading to a smooth alignment to the target track. The turning-point distance $\delta_0 \in \mathbb{R}^+$ is that distance, at which the bearing would point equally parallel and perpendicular to the target track (as $\tan^{-1} 1 = 45$ deg). Proposition 3 in [14] has a similar intention, with the difference that $\sigma\delta$ is replaced by $\pm \sin \delta$ and $\delta_0 \hat{=} L^{-1}$. Unlike the notation would suggest, Baayen and Ockel's [14] proposition 3 expresses equality of vector direction only.

One control task is to minimize a misalignment between the actual flight direction and this bearing. Let

$$e_\chi := \chi_{\text{cmd}} - \chi \quad (22)$$

be the attitude error, which gives a measure for this misalignment. Inserting into Eq. (18) and noting that $\sin \tan^{-1} x = x/\sqrt{x^2 + 1}$, $\cos \tan^{-1} x = 1/\sqrt{x^2 + 1}$ yields the dynamics of the geodesic distance

$$\dot{\delta} = -\frac{\dot{\rho}^K}{\sqrt{(\delta/\delta_0)^2 + 1}} \left(\frac{\delta}{\delta_0} \cos e_\chi + \sigma \sin e_\chi \right) \quad (23)$$

This essential equation shows that, for a vanishing attitude error $e_\chi \rightarrow 0$, a bearing angle, as chosen in Eq. (21), will let the geodesic distance decrease strictly for any $\delta > 0$ (as $\sigma^2 = 1 \forall \delta \neq 0$). Figure 14 shows the normalized phase plot of $\dot{\delta}/\dot{\rho}^K$ in the ideal case of $e_\chi = 0$. For $\delta/\delta_0 \gg 1$, Eq. (23) turns into $\dot{\delta} \approx -\dot{\rho}^K$, and hence, large geodesic distances decrease approximately linear, whereas for $\delta \rightarrow 0 \Rightarrow \dot{\delta} \approx -\dot{\rho}^K \cdot \delta/\delta_0$, an exponential decay, resulting in a smooth alignment with the target track, is guaranteed. The turning-point distance δ_0 plays an important role and can be used to adjust the

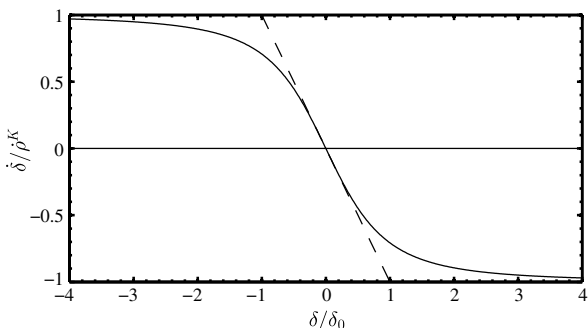


Fig. 14 Phase plot of Eq. (23) illustrating the dynamics of the geodesic distance δ .

interception behavior; larger values lead to a longer exponential-decay phase, which, on the one hand, makes the interception smoother but slower, whereas smaller values imply a late alignment with the long linear-approach phase.

2. Attitude Controller

To assure a decreasing geodesic distance δ , the error dynamics $\dot{e}_\chi = \dot{\chi}_{\text{cmd}} - \dot{\chi}$ are investigated in more detail. Assuming perfect feedback linearization, the desired rate of change of the flight direction $\dot{\chi}_d$ can be prescribed ($\dot{\chi} \equiv \dot{\chi}_d$), and so setting that to

$$\dot{\chi}_d := K_P e_\chi + \dot{\chi}_{\text{cmd}} \quad (24)$$

minimizes the attitude error exponentially

$$\dot{e}_\chi = -K_P e_\chi \quad (25)$$

This can easily be verified by inserting Eq. (24) back into the attitude-error dynamics, substituting $\dot{\chi}$ by $\dot{\chi}_d$ (which is valid as long as the feedback linearization is assumed perfect). With the proportional gain K_P chosen to let e_χ decrease sufficiently quick, but also to stay within a safe mode of operation ($r_{B,\max} \approx 3$ rad/s, $e_{\chi,\max} = 180$ deg = $\pi \Rightarrow K_P \approx 1$ s⁻¹), the two control laws, Eqs. (21) and (24), ensure a smooth alignment of the kite to the target track.

While the proportional compensator part of control law Eq. (24) predominantly minimizes the attitude error itself and is feasible using the IMU, the time derivative of the bearing $\dot{\chi}_{\text{cmd}}$ requires some additional attention. Differentiating Eq. (21) and using $(d/dt)(\tan^{-1} x) = \dot{x}/(x^2 + 1)$ yields

$$\dot{\chi}_{\text{cmd}} = \dot{\chi}_{C,K} + \underbrace{\frac{\sigma \dot{\delta}/\delta_0}{(\delta/\delta_0)^2 + 1}}_{=0 \Leftrightarrow \delta e_\chi = 0} \quad (26)$$

The second term is governed by the behavior of $\dot{\delta}$, and from Eq. (23), it follows that, for vanishing control errors δ , $e_\chi = 0$, this term also vanishes. As a consequence, even if no control errors are present, the control law Eq. (24) is commanding a certain yaw rate:

$$\dot{\chi}_d = \dot{\chi}_{C,K} \Leftrightarrow \delta, \quad e_\chi = 0$$

This is typical for tracking controllers, and $\dot{\chi}_{C,K}$, the time derivative of the course angle at \mathbf{K} , contains the shape and curvature of the target track. For highly curved trajectories, the controller will command high yaw rates to keep the kite on track. If $\dot{\chi}_{C,K}$ was omitted in the law, the kite would not maintain zero control error. Once on track, it would deviate from it again, building up new control errors, which in turn would be compensated by the controller. An oscillating and highly active control behavior would result.

D. Summary

The flowchart in Fig. 15 summarizes the control structure as it was implemented for the field tests. For reasons of readability, the computations of the geodesic distance δ and the course angle $\chi_{C,K}$ are grouped in a geometry block at the very left (see Sec. IV.A for details). The feedback linearization, based on the empirical yaw correlation, is preceded by the bearing and attitude loops, resulting in a cascaded control structure. The plant block would, in a simulation environment, usually be substituted by a multi-DOF kite model, such as the one proposed by Bosch [11]. However, as will be shown in Sec. V, this control structure was directly integrated into the technology-demonstrator software and hardware framework without excessive simulation, mainly due to the lack of validation of the available models.

The following list briefly recapitulates the essential parts of the control structure:

- 1) The geometry block encapsulates the determination of the closest point \mathbf{C} on the target trajectory according to Eq. (13), yielding

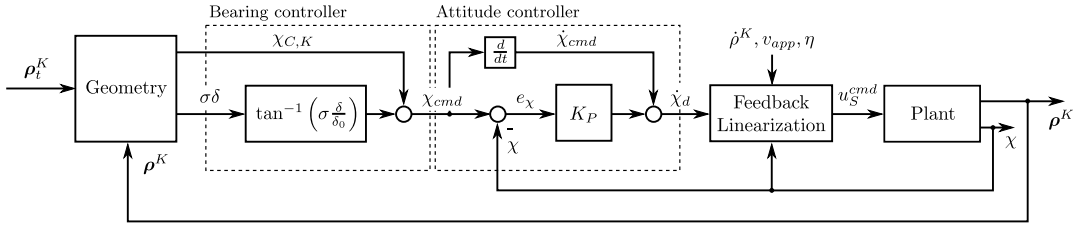


Fig. 15 Structure of the cascaded controller as implemented for the field tests.

both δ [Eq. (12)] and σ [Eq. (17)]. Moreover, it provides the track angle $\chi_{C,K}$ for the computation of the bearing.

2) The bearing controller, Eq. (21), determines a desired flight direction χ_{cmd} (bearing), designed to smoothly render the geodesic distance δ between the kite and the target trajectory to zero. The main tuning parameter is the turning-point distance δ_0 , which determines the geodesic distance from where on the kite will proceed from a linear approach to an exponential alignment to the track.

3) The attitude controller, Eq. (24), penalizes a misalignment between the actual flight direction and the bearing, expressed by the attitude error e_χ , using a proportional compensator with gain K_P . Its output is a desired rate of change of the flight direction $\dot{\chi}_d$. A baseline signal $\dot{\chi}_{cmd}$ is superimposed and mainly compensates for the shape of the target trajectory. If no control error is present, the attitude controller only commands this baseline signal, which — depending on the curvature of the target track — keeps the kite on path.

4) A feedback linearization, Eq. (20), based on the empirical steering correlation and a kinematical model of the kite, generates a steering input u_S , such that — in the ideal case of perfect system knowledge and all values measurable — the dynamics of the kite are compensated. As a result, the desired rate of change of the flight direction $\dot{\chi}_d$ will equate to the actual $\dot{\chi}$. This block could optionally be enhanced by an additional loop C to compensate for modeling imperfections.

5) The plant is, in this case, the real airborne kite power system, but would, in a simulation environment, be replaced by a suitable multi-DOF system model of the kite.

V. Experimental Results

Because of the lack of validated kite simulation models at the time this research was carried out, an intensive simulation of the controller was not possible. The focus was, in fact, to implement the control law and to integrate it into the available software and hardware structure of the technology demonstrator. This section, therefore, presents experimental results gathered in field tests, rather than simulation results.

First, the tracking-controller performance is presented, followed by a summary on the produced power. The last subsection is dedicated to examine and evaluate the various assumptions that have been made for control design (cf. Sec. III.C).

A. Implementation

The controller is integrated into the software and sensor framework of the technology demonstrator, and receives measurement data from an IMU/GPS combination, providing the heading angle ψ and tracking angle χ , position ρ^K , and velocity of the kite. For the determination of the apparent wind speed v_{app} , which is needed for the feedback linearization, a pitot tube is suspended in the bridle system.

The controller was tested under various weather conditions and with two LEI kites (a 25 m² and a 14 m² kite). For all test cases, a lemniscate of Bernoulli, which has been projected onto the unit sphere using Eq. (27), was used as the target trajectory.

All of the following results are taken from a test day in June 2012 at the Maasvlakte 2 site at the harbour of Rotterdam. An average ground wind speed of 9.7 ms⁻¹, with peak gusts up to 13.4 ms⁻¹, was measured during the day. Power cycles started at a tether length of

400 m, and the retraction phase was initiated when 600 m tether length was reached. The peak distance was 941.6 m.

B. Control Performance

Figure 16 shows the tracking performance for a series of five consecutive power cycles. The target trajectory is plotted bold and light gray, whereas the trace of the kite in spherical coordinates is a solid black line. The dotted lines indicate the approach and reel-in phases. After reel in, the kite reapproaches the target trajectory on the right-hand side of the wind window (except for one interception on the left), and aligns smoothly to the track. The controller was able to let the kite track the target trajectory within narrow bounds, and the results show a very good repeatability. An average geodesic distance of 28 mrad, which equates to approximately 14 m on 500 m tether length, was achieved.

However, an asymmetry between the left-hand side and the right-hand side can be observed; whereas the turns on the left are too narrow, the ones on the right are too wide. A known issue is that, in reality, a steering input $u_S = 0\%$ does not necessarily result in a nonyawing kite. As it was introduced in Sec. III.B, the steering input u_S is a relative measure for the amount of steering line that has been pulled respectively released on one wing-tip side. Due to twists and loose, improper or asymmetric windup of the steering lines onto the microwinchies, but also due to creep and elongation of those, the neutral steering position (i.e., at which the kite would not yaw) can be biased by some percentage, $u_{S,0} \approx \pm 5\text{--}10\%$. This asymmetry is difficult to determine beforehand, and has to be adjusted either manually during flight or by a loop for compensation of modeling imperfections (see also Sec. IV.B). As a result, the kite tends to permanently turn into one direction, and the control action is only superimposed, leading to sharper turns on the one, but wider turns on the other side. Although a PI compensator $C(s)$ (Sec. IV.B) was, in fact, active during the test, it was not able to fully compensate for this bias.

For the power cycle shown in Fig. 17, the neutral steering position has been adjusted as far as possible. Yet still, the control performance seems improvable — the kite overshoots at the end of the upstrokes and especially after the lower corners show wiggles and slight oscillations. Figure 18 shows both the commanded and the actual measured steering inputs, together with the geodesic distance δ during the approach (i.e., from the beginning at $\mathbf{q}^K \approx [-10^\circ, 44^\circ]^T$ up to $\mathbf{q}^K \approx [+17^\circ, 35^\circ]^T$). During the first 6–7 s, the geodesic distance decreases δ linearly, just as predicted by the control law, Eq. (23). Initially, the commanded steering input u_S^{cmd} evolves slow

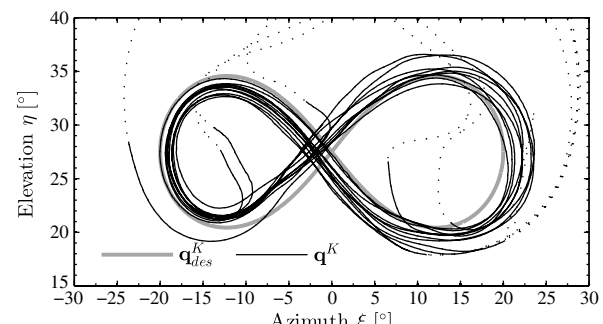


Fig. 16 Controller tracking performance on a 14 m² kite during five power cycles.

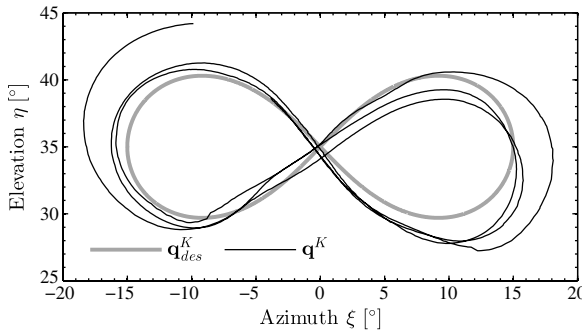


Fig. 17 Tracking performance during one power cycle (interception starting at the top margin).

enough for the winch actuators to follow, $u_S^{\text{cmd}} \approx u_S^{\text{meas}}$. Nonetheless, the kite overshoots the target track at $t = 7$ s. From $t = 5$ s, the controller demands a change in flight direction, which corresponds to the expected transition from the linear approach to the exponential alignment. Yet, the measured position of the steering actuators, u_S^{meas} , lags behind. Triggered by the overshoot, the controller commands a turn to the other side at $t = 7$ s; the sign of the u_S^{cmd} changes, corresponding to a turn into the other direction. The actual actuator position does track the set value, yet lagging behind, as the motors are not capable of turning fast enough. An oscillation results ($t = 7\text{..}14$ s), eventually leading to an increase in the geodesic distance.

This effect cannot be compensated for by just a PI loop $C(s)$, and an integral compensator may even deteriorate the control performance. As, depending on the gain, an integrator will quickly run into saturation when facing a time-delayed control error, it cannot effectively serve its purpose to, for example, minimize the effect of a steering bias anymore. This effect can be mitigated by tuning the control parameters, such that a less aggressive controller results (i.e., raise δ_0 and/or lower K_P). Faster steering winch motors will, of course, solve this issue, just as more advanced control laws, but these measures are a topic on itself.

C. Energy Production

Figure 19 shows the mechanical power P_m at the winch, measured during the same case, as shown in Fig. 16. The alternation between power generation during reel out and power consumption during reel in can nicely be observed. While, during the power phase, the average power was $\bar{P}_m^{\text{out}} = +9.64$ kW, reeling in consumed approximately $\bar{P}_m^{\text{in}} = -4.01$ kW. This results in a positive net power of around $\bar{P}_m = +5.37$ kW. The system in sum produces more energy than it consumes.

D. Miscellaneous Results

In Sec. III.C, the assumption of low tether sag was made. This assumption drastically simplified Eq. (7), and by that, facilitated the control law. The validity of this assumption will be briefly assessed in this subsection. Figure 20 shows the tether sag angles ϕ, θ during a

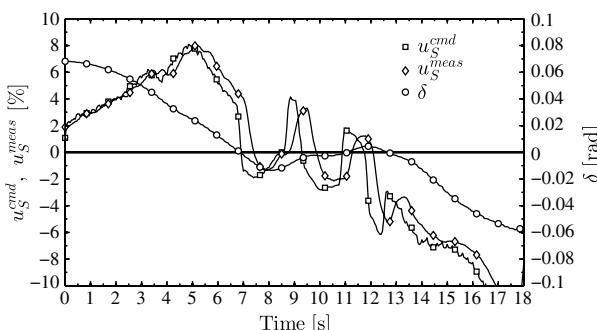


Fig. 18 Commanded and actual steering inputs and geodesic distance; flight of Fig. 17.

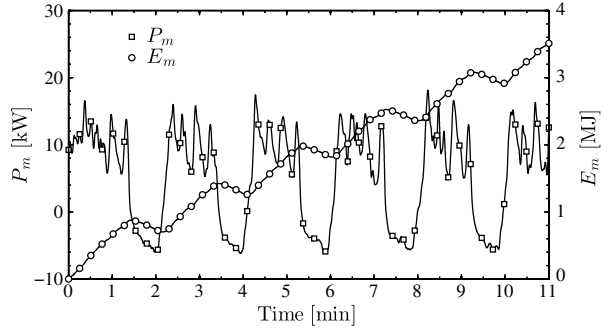


Fig. 19 Mechanical power P_m and energy E_m during the five power cycles (Fig. 16).

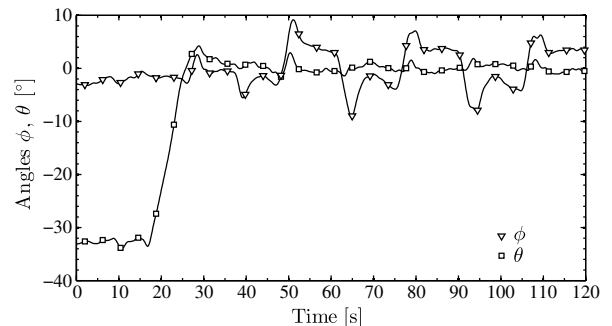


Fig. 20 Bank and pitch angles ϕ, θ during a power cycle at low wind speed.

power cycle of the 25 m² kite at a low wind speed of $v_w \approx 3.9$ ms⁻¹, 6 m height. In depowered mode ($u_p = 40\%$, $t < 30$ s), the kite pitches down, $\theta < -30$ deg, just as indicated in Fig. 8. The roll angle remains $\phi \approx 0$ deg, a typical situation for a depowered kite in idling position.

In powered flight, however, θ is almost constantly 0 deg, whereas ϕ shows an interesting evolution. After each corner of the eight-shaped trajectory, the roll angle quickly changes from $\phi \approx +4$ deg to -4 deg, with peaks at ± 7 deg. The kite dangles from one side to the other. This means that, while flying crosswind to one side, the kite maintains a roughly constant roll angle, as the mass of the KCU pulls it down over a lever arm of the length of the KCU cables. When the flight direction changes, the KCU falls, resulting in a peak roll angle, which diminishes to the aforementioned 4 deg.

Although this is generally an unfavorable circumstance (creep, wear, unsteady forces), the angles remain small even at low wind speeds, and neglecting them seems to be a valid assumption.

VI. Conclusions

The kinematic framework proves to be suitable for both the description of the kite's kinematics and the synthesis of the control law (i.e., the prescription of a target trajectory on a unit sphere and the definition of meaningful control values, such as the course and bearing angle, and the geodesic distance as an appropriate error signal). The close resemblance of the framework to concepts known from aerospace engineering facilitates dealing with the topic of tethered flying objects.

The presented empirical yaw correlation shows a very good fit and proves to be valid not only when compared to recorded measurement data, but also during controlled flight tests when being integrated into the flight controller. Its linear dependence to the apparent wind speed is surprising, as aerodynamic forces generally imply a square dependency. More analytical investigation and measurements could improve the understanding of the involved mechanisms; however, this is scheduled for future research. This could, in particular, improve the prediction of the now empirically determined parameters of this law to, for example, relate it to the power setting of the kite.

An improvement of the feedback linearization and, consequently, also of the whole control performance can be expected.

An analysis of the cascaded control laws reveals a linear decrease in time of the kite's distance to the target trajectory and a subsequent exponential alignment to it, leading to a smooth interception behavior. This is evident from both analytic investigation of the equations, but also from evaluating the measurement data from field tests. Even though only very few simulations were possible to assess the controller's performance beforehand, it showed convincing results in the various field tests. A stable operation was possible for several hours, and the controller thus proved its general capability for long-term tests.

The discrepancy between theoretically possible and practically achieved control performance can, on the one hand, be explained by the aforementioned uncertainties in the determination of the empirical-model parameters, but, on the other hand, also by the inability of the controller to cope with time delays and actuator constraints. Moreover, the fact that the neutral steering position (i.e., the steering command at which no yawing is observed) cannot be determined online turns out to be a nonnegligible flaw and significantly impairs the control performance. It is, therefore, necessary to improve the controller in terms of robustness and its ability to cope with hard nonlinearities, constraints, and sensor flaws. If possible, an acceleration of the microwinch motors, faster signal traveling times, and improved sensor (e.g., to measure the neutral steering position) would also improve the control performance.

The evaluation of measurement data from controlled flight tests shows a positive net-energy output of the system and additionally reveals that assumptions, such as a straight tether and low drift angles, are generally valid for the traction phase.

Appendix: Kinematic Framework

The following equations enable to convert between the Cartesian reference frame W and the azimuth/elevation-angle representation ($\mathbf{q}^T = [\xi, \eta]$) of a point \mathbf{K} on \mathbb{S}^2 :

$$\begin{aligned} (\rho)_W &= \mathcal{P}(\mathbf{q}) = \begin{bmatrix} \cos \eta \cdot \cos \xi \\ -\cos \eta \cdot \sin \xi \\ \sin \eta \end{bmatrix} \\ \mathbf{q} &= \mathcal{P}^{-1}[(\rho)_W] = \begin{bmatrix} -\tan^{-1}(\rho_y/\rho_x) \\ \sin^{-1}(\rho_z) \end{bmatrix} \end{aligned} \quad (\text{A1})$$

The time derivatives of the spherical coordinates as a function of the kite's velocity are found by differentiating Eq. (A1):

$$\dot{\mathbf{q}} = \frac{\partial \mathbf{q}}{\partial \rho} \cdot (\dot{\rho})_W = \begin{bmatrix} -\sin \xi / \cos \eta & -\cos \xi / \cos \eta & 0 \\ -\cos \xi \sin \eta & \sin \xi \sin \eta & \cos \eta \end{bmatrix} \cdot (\dot{\rho})_W \quad (\text{A2})$$

This can be further divided into

$$\dot{\mathbf{q}} = \begin{bmatrix} 0 & -1/\cos \eta & 0 \\ 1 & 0 & 0 \end{bmatrix} \cdot s \mathbb{T}_W \cdot (\dot{\rho})_W \quad (\text{A3})$$

Using $(\dot{\rho}^K)_S = \dot{\rho}^K \cdot [\cos \chi \ sin \chi \ 0]^T$ (cf. Fig. 9) turns Eq. (A3) into

$$\dot{\mathbf{q}} = \dot{\rho}^K \cdot \begin{bmatrix} -\sin \chi / \cos \eta \\ \cos \chi \end{bmatrix} \quad (\text{A4})$$

A coordinate transformation between the tangent-plane base S and a standard, $\{\mathbf{e}_r, \mathbf{e}_\theta, \mathbf{e}_\phi\}$ -base spherical coordinate system ($\theta^\circ, \varphi^\circ$ being inclination and polar angles, respectively) is achieved by

$$\cdot \mathbb{T}_S = \begin{bmatrix} 0 & 0 & -1 \\ -1 & 0 & 0 \\ 0 & 1 & 0 \end{bmatrix} \quad (\text{A5})$$

Acknowledgment

The financial support of the Rotterdam Climate Initiative is gratefully acknowledged.

References

- [1] MacCleery, B., "The Advent of Airborne Wind Power," *Wind Systems Magazine*, Jan. 2011, pp. 24–30.
- [2] Schmehl, R., "Kiting for Wind Power," *Wind Systems Magazine*, July 2012, pp. 36–43.
- [3] Fagiano, L., and Milanese, M., "Airborne Wind Energy: An Overview," *American Control Conference (ACC)*, 2012, American Automatic Control Council, Evanston, IL, 2012, pp. 3132–3143.
- [4] Ahmed, M., Hably, A., and Bacha, S., "High Altitude Wind Power Systems: A Survey on Flexible Power Kites," *XXth International Conference on Electrical Machines (ICEM)*, IEEE Publ., Piscataway, NJ, 2012, pp. 2085–2091.
doi:10.1109/ICEMach.2012.6350170
- [5] De Wachter, A., "Power from the Skies: Laddermill Takes Airborne Wind Energy to New Heights," *Leonardo Times: Journal of the Society of Aerospace Engineering Students VSV Leonardo da Vinci*, 2010, pp. 18–20.
- [6] Diehl, M., Magni, L., and De Nicolao, G., "Efficient NMPC of Unstable Periodic Systems Using Approximate Infinite Horizon Closed Loop Costing," *Annual Reviews in Control*, Vol. 28, No. 1, 2004, pp. 37–45.
doi:10.1016/j.arcontrol.2004.01.011
- [7] Ilzhöfer, A., Houska, B., and Diehl, M., "Nonlinear MPC of Kites Under Varying Wind Conditions for a New Class of Large-Scale Wind Power Generators," *International Journal of Robust and Nonlinear Control*, Vol. 17, No. 17, 2007, pp. 1590–1599.
doi:10.1002/(ISSN)1099-1239
- [8] Fagiano, L., "Control of Tethered Airfoils for High Altitude Wind Energy Generation," Ph.D. Thesis, Politecnico di Torino, Turin, Italy, 2009.
- [9] Canale, M., Fagiano, L., and Milanese, M., "KiteGen: A Revolution in Wind Energy Generation," *Energy*, Vol. 34, No. 3, 2009, pp. 355–361.
doi:10.1016/j.energy.2008.10.003
- [10] Breukels, J., "An Engineering Methodology for Kite Design," Ph.D. Thesis, Delft University of Technology, Delft, The Netherlands, 2011.
- [11] Bosch, A., "Finite Element Analysis of a Kite for Power Generation," M.S. Thesis, Delft University of Technology, Delft, The Netherlands, 2012.
- [12] Furey, A., "Evolutionary Robotics in High Altitude Wind Energy Applications," Ph.D. Thesis, University of Sussex, Brighton, East Sussex, U.K., 2011.
- [13] Erhard, M., and Strauch, H., "Control of Towing Kites for Seagoing Vessels," *IEEE Transactions on Control Systems Technology*, Vol. 21, No. 5, Sept. 2013, pp. 1629–1640.
doi:10.1109/TCST.2012.2221093
- [14] Baayen, J., and Ockels, W., "Tracking Control with Adaption of Kites," *IET Control Theory & Applications*, Vol. 6, No. 2, 2012, pp. 182–191.
doi:10.1049/iet-cta.2011.0037
- [15] Argatov, I., and Silvennoinen, R., "Asymptotic Modeling of Unconstrained Control of a Tethered Power Kite Moving Along a Given Closed-Loop Spherical Trajectory," *Journal of Engineering Mathematics*, Vol. 72, No. 1, 2012, pp. 187–203.
doi:10.1007/s10665-011-9475-3
- [16] Fechner, U., and Schmehl, R., "Design of a Distributed Kite Power Control System," *2012 IEEE International Conference on Control Applications*, IEEE Publ., Piscataway, NJ, 2012, pp. 800–805.
- [17] Breukels, J., and Ockels, W. J., "A Multi-Body System Approach to the Simulation of Flexible Membrane Airfoils," *Aerotecnica Missili & Spazio*, Vol. 89, No. 3, 2010, pp. 119–134.
- [18] de Groot, S. G., Breukels, J., Schmehl, R., and Ockels, W. J., "Modeling Kite Flight Dynamics Using a Multibody Reduction Approach," *Journal of Guidance, Control, and Dynamics*, Vol. 34, No. 6, 2011, pp. 1671–1682.
doi:10.2514/1.52686
- [19] Cook, M. V., *Flight Dynamic Principles: A Linear Systems Approach to Aircraft Stability and Control*, Butterworth-Heinemann, Oxford, England, U.K., 2007, Chap. 2.

- [20] Diebel, J., "Representing Attitude: Euler Angles, Unit Quaternions, and Rotation Vectors," Stanford Univ., Technical Rept., Stanford, CA, Oct. 2006, <http://www.swarthmore.edu/NatSci/mzucker1/e27/diebel2006attitude.pdf> [retrieved 16 July 2013].
- [21] Shuster, M. D., "A Survey of Attitude Representations," *Journal of the Astronautical Sciences*, Vol. 41, No. 4, 1993, pp. 439–517.
- [22] Loyd, M. L., "Crosswind Kite Power," *Journal of Energy*, Vol. 4, No. 3, 1980, pp. 106–111.
doi:10.2514/3.48021
- [23] Bullo, F., Murray, R. M., and Sarti, A., "Control on the Sphere and Reduced Attitude Stabilization," California Inst. of Technology TR-Caltech/CDS-95-005, Pasadena, CA, Jan. 1995, <http://resolver.caltech.edu/CaltechCDSTR:1995.CIT-CDS-95-005> [retrieved 18 Sept. 2013].
- [24] Narendra, K., and Valavani, L., "Stable Adaptive Controller Design Part I: Direct Control," *1977 IEEE Conference on Decision and Control Including the 16th Symposium on Adaptive Processes and A Special Symposium on Fuzzy Set Theory and Applications*, Vol. 16, IEEE Publ., Piscataway, NJ, 1977, pp. 881–886.
- [25] Kannan, S. K., and Johnson, E. N., "Model Reference Adaptive Control with a Constraint Linear Reference Model," *49th IEEE Conference on Decision and Control*, IEEE Publ., Piscataway, NJ, 2010, pp. 134–145.